MOL #70276

Inhibition of Neuronal Voltage-Gated Sodium Channels by Brilliant Blue G

Sooyeon Jo and Bruce P. Bean

Department of Neurobiology, Harvard Medical School, Boston MA 02115

1

Running title:

Sodium current inhibition by Brilliant Blue G

Address for correspondence:
Bruce P. Bean
Department of Neurobiology
Harvard Medical School
220 Longwood Avenue
Boston MA 02115
phone: (617)-432-1139
fax: (617)-432-3057
email: bruce_bean@hms.harvard.edu

10 Text pages; 8 Figures; 0 Tables; 39 references

Abstract: 250 words
Introduction: 325 words
Discussion: 1499 words

Abbreviations: BBG, Brilliant Blue G

Abstract

Brilliant blue G (BBG), best known as an antagonist of P2X7 receptors, was found to inhibit voltage-gated sodium currents in N1E-115 neuroblastoma cells. Sodium currents elicited from a holding potential of -60 mV were blocked with an IC_{50} of 2 µM. Block was enhanced in a use-dependent manner at higher stimulation rates. The voltage-dependence of inactivation was shifted in the hyperpolarizing direction, and recovery from inactivation was slowed by BBG. The most dramatic effect of BBG was to slow recovery from inactivation following long depolarizations, with 3 µM BBG increasing half-time for recovery (measured at -120 mV) from 24 msec to 854 msec following a 10-sec step to 0 mV. These results were mimicked by a kinetic model in which BBG binds weakly to resting channels (K_d 170 µM) but tightly to fast-inactivated channels (K_d 5 µM) and even more tightly (K_d 0.2 µM) to slow-inactivated channels. In contrast to BBG, the structurally-related food-coloring dye Brilliant Blue FCF had very little effect at concentrations up to 30 µM. These results show that BBG inhibits voltage-gated sodium channels at micromolar concentrations. Although BBG inhibition of sodium channels is less potent than inhibition of P2X7 receptors, there may be significant inhibition of sodium channels at BBG concentrations achieved in spinal cord or brain during experimental treatment of spinal cord injury or Huntington's disease. Considered as a sodium channel blocker, BBG is remarkably potent, acting with more than 10-fold greater potency than lacosamide, another blocker thought to bind to slow inactivated channels.

Introduction

The dye brilliant blue G (BBG), also known as Coomassie blue, is best known for its use in staining proteins in gel electrophoresis. However, BBG has also recently been recognized as a potential pharmacological agent, particularly for treating conditions involving neuronal death. Recent reports have shown that *in vivo* administration of BBG protects against amyloid-β-induced neuronal loss in a mouse model of Alzheimer's disease (Ryu and McLarnon 2008) and attenuates neuronal apoptosis and motor deficits in mouse model of Huntington's disease (Diaz-Hernandez et al., 2009). Recently, it was shown that BBG administered intravenously improves recovery and reduces local inflammatory responses in rats with spinal cord injury (Peng et al., 2009). The molecular targets of BBG are not completely understood. BBG is known to be a potent antagonist of the ATP-activated P2X7 receptor, blocking the receptor with an IC_{50} of 10-200 nM (Jiang et al., 2000), with 1,000-fold less potent effects on other P2X receptors. Possible effects on other types of ion channels have not been reported.

Structurally, BBG is a derivative of FD&C blue dye No.1 (also known as brilliant blue FCF), a widely used food dye which is considered to be non-toxic (Borzelleca et al., 1990). Possible toxicity of brilliant blue FCF, however, is still somewhat controversial, and recent reports indicate that application of brilliant blue FCF with other food dyes can induce neurotoxicity and inhibit hippocampal neurogenesis (Lau et al., 2006; Park et al., 2009). Thus the effects of brilliant blue FCF on neuronal function are also of considerable interest.

Here we present experiments showing that external BBG can inhibit neuronal TTX-sensitive sodium channels with micromolar affinity. BBG inhibition of sodium channels appears to involve a strong interaction with both fast-inactivated and slow-inactivated sodium channels. Although BBG inhibition of sodium channels is less potent than its inhibition of the P2X7 receptor, it is the most potent agent yet described for inhibiting sodium channels by interacting with the process of slow inactivation.

Materials and Methods

Mouse Neuroblastoma N1E-115 Cell Culture. Mouse N1E-115 neuroblastoma cells were purchased from American Type Culture Collection (Manassas, USA). Cells were grown in Dulbecco's modified Eagle's medium (ATCC) containing 10% fetal bovine serum (Sigma) and penicillin/streptomycin (Sigma) under 5% CO_2 at 37°C. For electrophysiological recording, cells were grown on coverslips for 12 to 24 h after plating.

RT-PCR. Total RNA was purified from 1.8×10^6 of N1E-115 cells using RNeasy® Mini Kit (Qiagen) and used for cDNA synthesis with random hexamers and M-MLV reverse transcriptase (Promega). Primer sets for each type of Nav channel were prepared as in Gao et al (2009). PCR reactions using RT reaction products were performed (94°C for 2 min; 25 cycles of 94 °C for 30 sec, 55 °C for 30 sec and 72 °C for 40 sec; 72 °C for 10 min).

Electrophysiology. Whole-cell recordings were obtained using patch pipettes with resistances of 2-3.5 MΩ when filled with the internal solution, consisting of 61 mM CsF, 61 mM CsCl, 9 mM NaCl, 1.8 mM $MgCl_2$, 9 mM EGTA, 14 mM creatine phosphate (tris salt), 4 mm MgATP, and 0.3 mM GTP (tris salt), 9 mM HEPES, pH adjusted to 7.2 with CsOH. The shank of the electrode was wrapped with Parafilm in order to reduce capacitance and allow optimal series resistance compensation without oscillation. Seals were obtained and the whole-cell configuration established with cells in Tyrode's solution (155 mM NaCl, 3.5 mM KCl, 1.5 mM $CaCl_2$, 1 mM $MgCl_2$, 10 mM HEPES, 10 mM glucose, pH adjusted to 7.4 with NaOH). To ensure complete dialysis with pipette solution, recordings began after 5 to 10 min after establishment of the whole-cell configuration. The amplifier was tuned for partial compensation of series resistance (typically 70-80% of a total series resistance of 4-10 MΩ), and tuning was periodically re-adjusted during the experiment. After establishing whole-cell recording, cells were lifted and moved in front of flow pipes containing an external solution consisting of 150 mM NaCl, 2.5 mM KCl, 2 mM $BaCl_2$, 30 μM $CdCl_2$, 1 mM $MgCl_2$, 10 mM HEPES, 13 mM Glucose, pH 7.4 (with NaOH). BBG (Sigma, 27815) or brilliant blue FCF (Pfaltz & Bauer Inc.) were used at concentrations between 3 μM to 100 μM. Currents were recorded at room temperature (21-23°C) with an Axopatch 200 amplifier and filtered at 5 kHz with a low-pass Bessel filter. Currents were digitized using a Digidata 1322A data

acquisition interface controlled by pClamp9.2 software (Axon Instruments) and analyzed using programs written in Igor Pro 4.0 (Wavemetrics, Lake Oswego, OR). Currents were corrected for linear capacitative and leak currents, which were determined using 5 mV hyperpolarizations delivered from the resting potential (usually −60 or −80 mV) and then appropriately scaled and subtracted. Statistical analyses were performed using IGOR Pro. Data are given as mean ± S.E.M., and statistical significance was assessed used Student's paired T-test.

Results

Brilliant Blue G (BBG) Inhibits Voltage-gated Sodium Channels.

Mouse-derived N1E-115 neuroblastoma cells are a convenient preparation for studying the pharmacology of voltage-gated sodium channels because they express sizeable TTX-sensitive sodium currents with only small potassium currents (e.g. Benzinger et al., 1999; Kondratiev et al., 2003; Errington et al., 2008). Cells were clamped in the whole-cell configuration, and peak current was evoked by 20-ms test pulses to 0 mV from a holding potential of either −60 mV or −80 mV, which span the range of typical resting potentials of mammalian neurons. At a holding potential of −60 mV, 3 μM BBG dramatically reduced the sodium current (reduction to $44 \pm 3\%$ of control) without an obvious effect on the kinetics of the current (Fig. 1A). The inhibition was partially reversible after removal of BBG (Fig. 1B). Fig. 1C shows the dose-dependence of inhibition of sodium current by BBG. The dose-response relationship for inhibition could be fit reasonably well by the equation $1/(1 + [BBG]/IC_{50})$, the relationship expected for 1:1 binding of drug to receptor, where IC_{50} is the half-blocking concentration. For test pulses delivered from a holding potential of −60 mV, sodium current was almost blocked completely by 30 μM BBG and the IC_{50} was 2.2 ± 0.3 μM (n = 3-5; Fig. 1C). When test pulses were delivered from a holding potential of −80 mV, block was significantly less potent, with an IC_{50} of 9.7 ± 1.3 μM (n = 3-5). The difference in blocking potency at the two different holding potentials can most easily be explained if BBG binds more tightly to the inactivated state of the sodium channel than to the closed "resting" state. At −80 mV, only about 10% of the channels are in the inactivated state, while at −60 mV, about 75% of the channels are

6

in the inactivated state (Fig. 4A). As expected from this, the blocking potency was even lower (IC$_{50}$ of 171 ± 1.3 µM (n = 4) with a holding potential of -120 mV, where channels should be almost exclusively in the resting state. As will be shown, the tighter binding to inactivated channels at more depolarized holding potentials likely involves binding to distinct fast and slow inactivated states with different affinities.

These results show that BBG inhibits the sodium channels present in N1E-115 cells with micromolar affinity at physiological resting potentials. To determine what type of sodium channels are being targeted in these experiments, we performed RT-PCR to determine which sodium channels are expressed in N1E-115 cells. We found expression of the neuronal sodium channel Nav1.3 with no detectable expression of other isoforms (Fig. 1D).

BBG Produces Use-Dependent Block of Sodium Channels.

We next tested for possible use-dependent block of sodium channels by BBG. Under control conditions, there was relatively little change in the sodium current if the stimulation rate was abruptly increased from 0.05 Hz to 3 Hz stimulation (current in the last pulse after one minute of 3 Hz stimulation was 93 ± 1% compared to the first; n = 4). However, in the presence of 3 µM BBG, there was substantial use-dependent block during 3 Hz stimulation such that current in the last pulse was reduced to 65 ± 3% (n = 4) of the current elicited by the first pulse (Fig. 2). When the stimulation rate was returned to 0.05 Hz, the current slowly recovered. After one minute of 0.05 Hz stimulation, the current in the presence of BBG recovered to 97 ± 1% of the original control current (n = 4). Recovery could be fit with an exponential time-course with time constant 17 ± 6 sec.

BBG Alters Voltage Dependence of Fast Inactivation but not Activation.

Application of 3 µM BBG reduced the peak currents at all test potentials equally (Figure 3A, B). The plot of peak conductance versus test voltage could be fit fairly well by a Boltzmann function (Figure 3C), and there was no significant difference in the voltage for half-activation in control (−28.8 ± 1.7 mV) and with 3 µM BBG (−29.1 ± 2.2 mV; n = 4, P = 0.7, paired t-test).

Figure 4 shows the effect of BBG on the voltage-dependence of inactivation, determined using 1-second steps to various voltages followed by a test pulse to 0 mV to assay sodium channel availability. BBG produced a negative shift in the voltage-

dependence of inactivation. The effect of BBG on inactivation was dose-dependent, with larger concentrations producing a larger hyperpolarizing shift in the midpoint (Fig. 4A). The voltage-dependence of inactivation could be fit well by a Boltzmann function. In control, the mid-point of inactivation (V_h) was -66 ± 1 mV and the slope factor (k) was 6.2 ± 0.2 (n = 4). In the presence of 3 μM BBG, the mid-point of inactivation shifted in the hyperpolarizing direction ($V_h = -73 \pm 1$ mV; $P = 0.0004$) and the slope factor increased slightly ($k = 7.3 \pm 0.3$; $P = 0.004$). These effects were progressively larger for larger concentrations of 30 μM BBG ($V_h = -80 \pm 1$ mV ($P = 0.0004$), $k = 8.8 \pm 0.4$ ($P = 0.006$)) and 100 μM BBG ($V_h = -87 \pm 1$ mV ($P < 0.0002$), $k = 9.3 \pm 0.4$ ($P = 0.004$), paired t-test for n = 4 for all).

In addition to the shift of the voltage-dependence of inactivation, BBG reduced the maximal current elicited with the most negative conditioning voltages tested, with an average of 65 ± 6 % block by 100 μM BBG with a 1-sec conditioning pulse to -120 mV. This is substantially more block than was produced by 100 μM BBG applied at a steady holding potential of -120 mV (34 ± 4 %; Fig. 1 C). This difference suggests that a 1-sec conditioning pulse is not long enough to reach a steady-state condition. Therefore, most subsequent experiments on the voltage-dependence and kinetics of BBG effects were done using longer conditioning pulses (Figs. 5 and 6).

BBG Slows Recovery from Inactivation

Many compounds that produce a shift in the steady-state inactivation curve of sodium channels and show use-dependent potentiation of block also produce slowing of recovery from inactivation (e.g. Bean et al., 1983; Kuo et al., 1997). Accordingly, we examined the effect of BBG on the time-course of recovery from inactivation. In a first series of experiments (Fig 5A), we examined recovery at a holding potential of -80 mV after a 20-msec prepulse to 0 mV. The time-course of recovery in control could be fit by the sum of two exponentials, a dominant fast phase with a time constant of about 5 msec and a small slow phase with a time constant of about 50 msec. In collected results in control, the fast phase was 89 ± 1% of the total and had a time constant of 4.9 ± 0.4 msec and the slow phase had an average time constant of 58 ± 11 msec (n = 4). Recovery was slower in 3 μM BBG, but not dramatically. With 3 μM BBG, the fast phase was slower (time constant of 7.2 ± 0.8 msec, $P = 0.02$) and the slow phase was also slower (time

constant of 94 ± 16 msec, $P = 0.012$). The relative amplitude of the slow phase was greater with BBG (15 ± 2 % with BBG compared to 11 ± 0.8 % in control, $P = 0.06$; n = 4).

Figure 5B shows the effect of BBG on recovery from inactivation using a different protocol in which inactivation was induced by a much longer (10-sec) depolarization to 0 mV. To avoid the complication that with a holding potential of -80 mV channels are already significantly inhibited by BBG during the first pulse to 0 mV, we used a holding potential of -120 mV, where steady-state resting block is minimal. The effects of BBG on recovery following a 10-sec prepulse were very dramatic. In control, recovery had a biphasic time course, with rapid recovery of about 75% of the current over the first 50-100 msec followed by a much slower phase of recovery that continued up to 6 seconds. If the total recovery in control was fit by the sum of two exponentials, the faster phase had an average time constant of 6 ± 2 msec and made up 54 ± 2 % of the total recovery, while the slower phase had an average time constant of 300 ± 5 msec and made up 46 ± 2 % (n = 4) of the total recovery. However, fits with two exponentials were not very good, and the slower phase of recovery clearly had multiple components, including components much slower than a second. Fitting the recovery from 1 to 6 seconds yielded a much slower time constant (2.8 ± 0.3 sec, making up 7 ± 1 % of the total recovery).

The presence of slow components in recovery following long depolarizations to 0 mV suggests that a substantial fraction of channels enter a "slow" inactivated state from which recovery is much slower than for the conventional inactivated state reached with brief depolarizations. Such a component of slow inactivation is seen for most, if not all, sodium channels (Rudy, 1978; reviewed by Vilin and Ruben, 2001; Goldin, 2003; Ulbricht, 2005) and has been previously described for sodium channels in N1E-115 cells (Errington et al., 2008) .

In the presence of BBG, recovery following a 10-sec depolarization to 0 mV was dramatically slowed. Almost all of the recovery occurred with slow kinetics. The fraction of current that had recovered after 100 msec at -120 mV was reduced from 73 ± 3 % in control to 16 ± 3 % with 3 μM BBG, 9 ± 3 % with 30 μM BBG, and 5 ± 3% with 100 μM BBG (n = 4 for all). The slowing of recovery can also be quantified by comparing the time for half-recovery, which was 24 ± 6 msec in control, 854 ± 154 msec in 3 μM BBG,

1025 ± 97 msec in 30 µM BBG, and 1066 ± 150 msec in 100 µM BBG. If the recovery from 1 to 6 seconds was fit with an exponential, the time constant of this component slowed from 2.8 ± 0.3 sec (accounting for 7 ± 1 % of the total recovery) in control to 6.3 ± 0.2 sec (54 ± 2 % of the total) with 3 µM BBG, 6.6 ± 0.3 sec (59 ± 2 % of the total) with 30 µM BBG, and 5.8 ± 0.8 sec (56 ± 5 % of the total) with 100 µM BBG. Thus, the occupancy of the most slowly-recovering states was already nearly saturated with 3 µM BBG and showed no change between 30 µM and 100 µM BBG. The powerful effect of even 3 µM BBG to put the great majority of channels in slowly-recovering states following 10-second pulses to 0 mV suggests that BBG binds tightly to a state reached during long depolarizations, from which recovery is slow . Also, when bound by BBG, such channels recover even more slowly ($\tau \sim 6$ sec) than the slowest component of normal recovery from slow inactivation ($\tau \sim 3$ sec).

Voltage Dependence of Slow Inactivation.

The anti-epileptic agent lacosamide was proposed to inhibit sodium channel activity by affecting slow inactivation without affecting fast inactivation (Errington et al., 2008; Sheets et al., 2008). We explored the possibility that BBG might interact with slow inactivation using pulse protocols similar to those previously used to study lacosamide (Errington et al., 2008). To evaluate the voltage-dependence with which channels enter slow inactivation, a 5-second prepulse to various voltages was followed by a test pulse to 0 mV delivered after a 100-msec recovery interval at −120 mV (Fig. 6A). This interval should allow complete recovery from fast inactivation, so that the test pulse assays channels remaining in a slow inactivated state. In control, on average 31 ± 6 % (n = 4) of the channels were in slowly recovering states following a 5-sec prepulse to +20 mV (and 100 msec recovery at −120 mV). In the presence of BBG, there was a dramatic increase in the fraction of channels recovering slowly after 5-second prepulses. On average 84 ± 6 % channels recovered slowly after a 5-sec pulse to +20 mV in the presence of 3 µM BBG ($P = 0.0027$, n = 4). In addition, the apparent voltage-dependence of slow inactivation shifted in the hyperpolarizing direction with BBG, so that the midpoint changed from −31 ± 4 mV in control (n = 4) to −55 ± 1 mV in 3 µM BBG (n = 4; $P = 0.0077$). The effects of 30 µM and 100 µM BBG were even more dramatic, with 90 ±

10

2 % of the channels immobilized by a 5-sec pulse to +20 mV with 30 μM (P = 0.0015, n = 3) and 93 ± 4 % by 100 μM BBG (P = 0.0001, n = 3). The midpoint also shifted more negatively in higher concentrations of BBG, with a midpoint of −80 ± 2 mV in 30 μM BBG (n = 3; P = 0.0036) and −90 ± 3 mV in 100 μM BBG (n = 3; P = 0.0007).

In principle, the apparent enhancement by BBG of slow-inactivated channels in the experiments of Fig. 5B and 6A could originate from BBG binding to fast-inactivated states, if recovery from BBG-bound fast-inactivated states was slow (e.g. if BBG unbinding was slow). To explore whether BBG entry into slowly-recovering states represents binding to fast-inactivated or slow-inactivated states, we compared the kinetics of BBG-enhanced entry into slowly recovering states at two different voltages, -50 mV and 0 mV. Fast inactivation is nearly complete at both voltages, but in control there is little slow inactivation at -50 mV but substantial slow inactivation at 0 mV (Fig. 6A). Therefore a difference in BBG action would be suggestive of interaction with slow inactivated states. Figure 6B shows the results of this experiment. The time course with which channels enter slowly-recovering states at -50 mV was compared with that at 0 mV, both in control and in the presence of BBG. A step to either -50 mV or 0 mV varying in length from 1 to 16 seconds was given from a holding potential of -120 mV. A 100-msec interval at -120 mV then allowed for recovery of fast-inactivated channels, and the fraction of channels remaining in slowly-recovering states was assayed by a pulse to 0 mV. In control, only a small fraction of channels entered slow inactivation at -50 mV (on average, 15 ± 2 % after 16 seconds at -50 mV). A larger fraction of channels entered slow inactivation at 0 mV (on average, 42 ± 3 % after 16 seconds at 0 mV). Entry into the slow inactivated state was slow even at 0 mV, occurring with an average time constant of 10 ± 2 seconds.   In the presence of BBG, a much larger fraction of channels became slowly-recovering at both -50 mV and 0 mV, and entry into slowly-recovering states was faster. With 3 μM BBG, 70 ± 4 % of channels were in slowly-recovering states after 16 seconds at -50 mV, and the time constant of entry was of 6.8 ± 1.3 seconds at -50 mV. With 3 μM BBG at 0 mV, development of slow-inactivation was much more complete (88 ± 3 % of channels after 16 seconds) and also much faster (time constant of 1.7 ± 0.2 seconds). The effects of 30 μM and 100 μM BBG were more profound at both conditioning voltages but showed less dramatic differences between the two voltages. With 30 μM BBG, slow

11

inactivation developed with a time constant of 1.4 ± 0.2 seconds at -50 mV (to 80 ± 0 %
completion) and with a time constant of 0.8 ± 0.04 seconds at 0 mV (to 90 ± 0 %
completion). Development of slow inactivation with 100 µM BBG was somewhat faster
and more complete: a time constant of 0.9 ± 0.06 seconds at -50 mV (to 88 ± 3 %
completion) and a time constant of 0.6 ± 0.04 seconds at 0 mV (to 100 ± 4 % completion).
The time constants give an estimate of the speed of development of the fraction of
slowly-recovering channels, but it should be noted that the development of slow
inactivation with 30 and 100 µM BBG was actually biphasic and imperfectly
approximated by single exponential fits.

Model for BBG Binding to Resting and Inactivated States

We tested several different kinetic models for BBG interaction with various gating states
of the sodium channel. To account for the experimental data with different BBG
concentrations, we found that it was necessary to assume that BBG binds to both fast
inactivated states and slow inactivated states, with much higher-affinity binding to slow
inactivated states. Figure 7 shows a simple model with a single fast inactivated state and a
single slow inactivated state that was able to simulate most of the experimental results. In
the model, BBG is assumed to bind weakly to the non-inactivated resting state of the
channel (K_d 170 µM), more tightly to the fast inactivated state (K_d 5 µM), and even more
tightly to a slow inactivated state (K_d 0.2 µM). The unbinding rate of BBG from both fast
inactivated and slow inactivated channels is slow enough that there is little recovery in
100 msec at -120 mV; thus, the slowly-recovering fraction of channels includes the states
S, S-BBG, and I-BBG. The entry of channels into these slowly recovering states during a
long depolarization to 0 mV occurs mainly by way of BBG binding to the fast-inactivated
state I, followed by movement from I-BBG to S-BBG. There is much less movement of
channels from I to S to S-BBG, because the rate constant for I to S is quite slow (but the
rate constant for I-BBG to S-BBG is faster, in a manner consistent with preserving
microscopic reversibility).

We also considered a simpler model with a single fast inactivated state to which BBG
binds and unbinds slowly, thus giving large slow phases in both development and
recovery. This simpler model could give a reasonable approximation for the kinetics of
recovery following long depolarizations. However, it could not explain the large

differences in the amount of slowly-recovering block after conditioning pulses to 0 mV compared to -50 mV. Since fast inactivation is nearly complete at -50 mV, the fraction of channels inactivated and available to bind tightly to BBG is nearly the same at -50 mV and 0 mV, and the degree of BBG block from binding to a single fast inactivated state is predicted to be nearly the same at -50 mV and 0 mV. In contrast, in the experimental data, block by 3 μM BBG is much more profound at 0 mV than at -50 mV. This is explained by the model that includes the slow inactivated state, because at 0 mV a greater fraction of channels is in the slow inactivated state than at -50 mV. As these slow inactivated channels bind BBG with high affinity, block is more profound at 0 mV than at -50 mV.

The model did not match the experimental data perfectly. Most significantly, the model did not produce as large a difference as was present experimentally in the kinetics of development of block by 3 μM BBG with a conditioning prepulse to 0 mV compared to -50 mV. The model of a single fast inactivated state and a single slow inactivated state is highly simplified compared to the actual behavior of sodium channels, which have multiple fast-inactivated states reached from different closed states (Kuo and Bean, 1994) and very likely multiple slow inactivated states as well (Karoly et al., 2010). Also, for simplicity we connected the slow inactivated state sequentially to the fast inactivated state, so that channels are in one or the other but not both. In fact, however, the fast inactivation gate can move independently of whether channels are slow inactivated (Vedantham and Cannon, 1998), which would give considerably more complex models (Vedantham and Cannon, 1998; Karoly et al., 2010). Models with additional fast or slow inactivated states might better predict the much faster kinetics of BBG action during conditioning pulses to 0 mV compared to -50 mV.

Brilliant Blue FCF Has Little Effect on Sodium Channels

We next considered the effects on sodium channels of the structurally related dye Brilliant Blue FCF. Although BBG is a derivative of Brilliant Blue FCF, the effects of Brilliant Blue FCF were far smaller than those of BBG. Fig. 8 shows the effects of Brilliant Blue FCF applied at 30 μM, ten times the standard concentration of BBG that we used for experiments with the same voltage protocols. The effects of 30 μM Brilliant Blue FCF were far smaller than 3 μM BBG. At 30 μM, Brilliant Blue FCF had only very little effect on peak sodium current (Fig. 8A). There was also only a very small effect on

the voltage dependence of fast inactivation, with shift of 2 mV with 30 µM Brilliant Blue

FCF (control: V_h= −66 mV ± 0.6, k=6.6 ± 0.13; Brilliant Blue FCF: V_h= −68.4 mV ± 1.1,

k=6.8 ± 0.3 (n=3); P=0.05 for V_h, P=0.5 for k), much less than the 14 mV shift seen with

30 µM BBG. In addition, Brilliant Blue FCF had little effect on the magnitude or kinetics

of slow inactivation. The fraction of channels available following a 5-second prepulse to

−10 mV (and a 1 sec recovery at −80 mV) was 72 ± 3% in control and decreased only

slightly in 30 µM Brilliant Blue FCF, to 67 ± 2% Fig. 8C (P = 0.183, n = 3). By

comparison, with the same voltage protocol, 3 µM BBG produced a change from 70 ±

3% available in control to 36 ± 4% in 3 µM BBG (P = 0.0001, n = 4). In addition, the

kinetics of recovery from slow inactivation were little affected by 30 µM Brilliant Blue

FCF (Fig 8D).

Discussion

We found that BBG inhibits voltage-gated sodium channels at low micromolar concentrations, with an IC_{50} of about 2 μM when applied at -60 mV, a typical neuronal resting potential. The most dramatic effect of BBG was to promote entry of sodium channels into inactivated or drug-bound states from which recovery is slow. BBG at 3 μM enhanced the fraction of channels that recovered slowly after a 16-sec depolarization to -50 mV by more than 4-fold, from 15% to 70%.

We could model the effects of BBG reasonably well by assuming a moderately high affinity binding to a fast inactivated state (K_d 5 μM) and very high affinity binding to a slow inactivated state (K_d 0.2 μM). As noted by Karoly et al. (2010), it is difficult to distinguish between models in which drugs bind with high affinity to slow inactivated states and models in which drugs bind only to fast inactivated states, but with slow kinetics. Our model includes binding to both fast inactivated channels and slow inactivated channels, and both seemed to be required for adequate modeling of the experimental results. With binding exclusively to slow inactivated channels, it was impossible to model the fact that development of slowly-recovering block at 0 mV is so much faster with BBG (τ~ 2 seconds with 3 μM BBG and 0.8 second with 30 μM BBG) than development of normal slow inactivation (τ ~ 10 seconds), because if drug binds only to slow inactivated channels, entry of channels into the slow inactivated state is rate-limiting. Also, it was impossible to produce the large shifts in inactivation measured with 1-sec conditioning pulses if BBG binding was exclusively to slow inactivated states, because entry and recovery from slow inactivated states is so slow.

Models in which BBG binds (and unbinds) exclusively to fast-inactivated channels with relatively slow kinetics were much better able to mimic the experimental results, including the shifts in 1-sec inactivation curves and the concentration-dependent development of slow-recovering channels. Also, as noted by Karoly et al. (2010), models in which BBG binding was exclusively to the fast inactivated state could predict the concentration-dependent shift in the apparent voltage-dependence of slow inactivation (Fig. 6A), because drug-bound fast-inactivated channels recover slowly and can mimic enhanced slow inactivation. However, models in which BBG binds exclusively to fast inactivated channels failed in two predictions. First, a binding affinity to fast inactivated

channels (~5 µM) that accounted for the degree of shift in 1-sec inactivation curves predicted much too little effect of 3 µM BBG on the fraction of channels recovering slowly after 10-sec at 0 mV (Fig 5B). Second, exclusive binding to fast inactivated channels predicted nearly identical time-course of block at -50 mV and 0 mV, because fast inactivation is nearly complete at both voltages. This is very different from the experimental results (Fig. 7). The much more dramatic effects of BBG at 0 mV compared to -50 mV can be explained by additional, tighter binding to slow inactivated channels, because slow inactivation is much more pronounced at 0 mV compared to -50 mV. However, even the model with BBG binding to both fast and slow inactivated states in Fig. 7 failed to account quantitatively for the degree to which BBG action at 0 mV is faster than at -50 mV.

The hypothesis that BBG binds to slow as well as fast inactivated states can account for the observation that the BBG-induced shift in the midpoint of inactivation determined with 1-second pulses is accompanied by an increase in the slope factor (Fig. 4). This effect is not explained by models with a single inactivated state, which predict a parallel shift of the inactivation curve with no change in slope (Bean et al., 1983) – as seen experimentally with lidocaine (Bean et al., 1983), phenytoin (Kuo and Bean, 1994), carbamazepine (Kuo, 1998), and lamotrigine (Kuo, 1998). Because the interaction of BBG with slow inactivated states is not in steady-state during 1-sec conditioning pulses, progressive recovery from slowly-recovering states at increasingly negative voltages produces a more shallow curve.

The specific affinities of BBG binding to fast and slow inactivated states predicted by the model depend on its details, but the experimental results leave no doubt that binding of BBG to combined fast and slow inactivated states must occur with high enough affinity that binding is nearly saturated by 3 µM BBG, which produced nearly saturating effects on recovery following 10-sec depolarizations (Fig 5B). Thus, the K_D for binding to inactivated channels must be at least as low as ~0.5 µM. Interestingly, this is much tighter binding to inactivated channels than for many other well-studied sodium channel blockers, including lidocaine (10 µM; Bean et al, 1983), lamotrigine (9 µM; Kuo and Lu, 1997), phenytoin (6 µM; Kuo and Bean, 1994) and carbamazepine (25 µM; Kuo et al., 1997).

The promotion of slow recovery after long depolarizations by BBG is similar to effects of lacosamide, which was proposed to have a selective interaction with slow inactivation (Errington et al., 2008). However, the effects of BBG were much more potent, with 3 μM BBG producing similar effects on slow recovery as 100 μM lacosamide (Errington et al., 2008). Unlike lacosamide, which produced no shift in inactivation studied with 500-msec conditioning steps (Errington et al., 2008), BBG produced large shifts (>20 mV) in inactivation studied with 1-sec depolarizations (Fig. 4). This difference is consistent with binding of BBG to both fast inactivated and slow inactivated channels but lacosamide binding exclusively to slow inactivated channels. However, it is difficult to rule out the possibility that lacosamide also binds to fast inactivated states but with slower kinetics than BBG (cf. Karoly et al., 2010).

Mechanistically, fast inactivation involves binding of a region of the III-IV intracellular linker to the intracellular pore region (West et al., 1992) while slow inactivation is a distinct mechanistic process that can occur in parallel with fast inactivation (Vedantham and Cannon, 1998) and may involve conformational changes of the outer pore region of the channel (e.g. Struyk and Cannon, 2002; Goldin, 2003; Xiong et al., 2006). Therefore, high-affinity binding of BBG to slow inactivated states may occur to an external binding site distinct from that accessed by drugs such as lidocaine, phenytoin and carbamazepine, generally thought to bind to an internal region of the pore lumen (Ragsdale et al., 1996; Yarov-Yarovoy et al., 2001; Lipkind and Fozzard, 2010; but see Yang and Kuo, 2002)

BBG is a derivative of FD&C blue dye No. 1 (brilliant blue FCF) which is a commonly used food additive and is generally regarded as having little toxicity (Borzelleca et al., 1990; Remy et al., 2008). Our results show that in contrast to BBG, brilliant blue FCF had very little effect on sodium channels even when applied at 10-fold higher concentrations. This is reassuring given the wide-spread ingestion of brilliant blue FCF.

BBG administration potently inhibits amyloid β-induced neuronal loss (Ryu and McLarnon 2008) and attenuates the motor coordination deficit in mouse models of Huntington's disease (HD) mice (Diaz-Hernandez et al., 2009). Recently, Peng and colleagues demonstrated that BBG improves recovery after spinal cord injury (SCI). In

their study, rats receiving 10 mg/kg or 50 mg/kg BBG (injected intravenously), had average BBG concentrations of 9.94 ± 8.32 μM or 43.59 ± 14.64 μM within spinal cord tissue. These are well above the IC_{50} of 2 μM for blocking sodium channels, suggesting that the treatments may effectively inhibit sodium channels in the injured spinal cord tissue in addition to more potent inhibition of P2X7 receptors (Jiang et al., 2000).

Sodium channel blockers are of current interest for the treatment of neuropathic pain (Waxman et al., 1999; Finnerup et al., 2002; Wood et al., 2004; Cummins et al., 2007). The voltage-gated sodium channel $Na_V1.3$ is upregulated after traumatic spinal cord injury, and targeted antisense knock-down of $Na_v1.3$ significantly reduces hyperexcitability of dorsal horn sensory neurons and pain-related behavior after spinal cord injury, implying that $Na_v1.3$ acts in amplification and generation of pain signals (Waxman and Hains 2006). In fact, $Na_V1.3$ shows unique expression, with relatively high-level expression in embryonic rat dorsal root ganglion (DRG) neurons but diminished expression in the normal adult spinal cord (Furuyama et al., 1993; Felts et al., 1997) until being up-regulated by injury. Interestingly, $Na_v1.3$ is the main sodium channel expressed in the N1E-115 cells we used as an assay system, so the results with these cells may be relevant to the possible block of $Na_v1.3$ channels in damaged spinal cord.

In summary, our results suggest that the P2X7 antagonist BBG also potently blocks voltage-gated sodium channels. BBG inhibition appears to involve high-affinity binding to both fast and slow inactivated states, and BBG acts with higher affinity than many classic sodium channel blockers, including lidocaine, phenytoin, carbamazepine, and lacosamide.. The lack of effect by the structurally related dye brilliant blue FCF offers the future possibility of determining the structural elements of BBG that mediate high-affinity interaction with both fast and slow inactivated states and of designing even more potent inhibitors that act in this way.

Authorship Contributions

Research design: Jo and Bean

Conducted experiments: Jo

18

Performed data analysis: Jo and Bean

Wrote manuscript: Jo and Bean

References

Bean BP, Cohen CJ, Tsien RW. (1983) Lidocaine block of cardiac sodium channels. *J Gen Physiol* **81:**613–642.

Benzinger RG, Tonkovich GS, Hanck DA. (1999) Augmentation of recovery from inactivation by site-3 Na channel toxins. A single-channel and whole-cell study of persistent currents. *J Gen Physiol* **113:**333–346.

Borzelleca JF, Depukat K, and Hallagan JB (1990) Lifetime toxicity/carcinogenicity studies of FD & C Blue No. 1 (brilliant blue FCF) in rats and mice. *Food Chem Toxicol* **28:**221–34.

Cummins TR, Sheets PL, and Waxman SG (2007) The roles of sodium channels in nociception: implication for mechanisms of pain. *Pain* **30:**243–257.

Díaz-Hernández M, Díez-Zaera M, Sánchez-Nogueiro J, Gómez-Villafuertes R, Canals JM, Alberch J, Miras-Portugal MT, and Lucas JJ (2009) Altered P2X7-receptor level and function in mouse models of Huntington's disease and therapeutic efficacy of antagonist administration. *FASEB J* **23:**1893–906.

Errington AC, Stohr T, Heers C, and Lee G (2008) The inverstigational anticonvulsant lacosamide selectively enhances slow inactivation of voltage-gated sodium channels. *Mol Phamacol* **73:**157–169.

Felts PA, Yokoyama S, Dib-Hajj S, Black JA, and Waxman SG (1997) Sodium channel alpha-subunit mRNAs I, II, III, NaG, Na6 and hNE (PN1): different expression patterns in developing rat nervous system. *Brain Res Mol Res* **45:**71–82.

Finnerup NB, Sindrup SH, Bach FW, Johannesen IL, and Jensen TS (2002) Lamotrigine in spinal cord injury pain: a randomized controlled trial. *Pain* **96:** 375–383.

Furuyama T, Morita Y, Inagaki S, and Takagi H (1993) Distribution of I, II and III subtypes of voltage-sensitive Na+ channel mRNA in the rat brain. *Brain Res Mol Brain Res* **17:**169–173.

Gao N, Lu M, Echeverri F, Laita B, Kalabat D, Williams ME, Hevezi P, Zlotnik A, Mayer BD (2009) Voltage-gated sodium channels in taste bud cells. *BMC Neurosci* **12:**12-20.

Goldin AL (2003) Mechanisms of sodium channel inactivation Curr Opin Neurobiol. 13:284- 90.

Jiang LH, Mackenzie AB, North RA, and Surprenant A (2000) Brilliant blue G selectively blocks ATP-gated rat P2X(7) receptors. *Mol Pharmacol* **58:**82–88.

Karoly R, Lenkey N, Juhasz AO, Vizi ES, Mike A. (2010) Fast- or slow-inactivated state preference of Na+ channel inhibitors: a simulation and experimental study. PLoS Comput Biol. 6: e1000818.

Kondratiev A, Hahin R, Tomaselli GF. (2003) Isoform-specific effects of a novel BmK 11(2) peptide toxin on Na channels. *Toxicon* **41:**269–276.

Kuo CC. (1998) A common anticonvulsant binding site for phenytoin, carbamazepine, and lamotrigine in neuronal Na+ channels. Mol Pharmacol. 54:712-721.

Kuo CC, Bean BP. (1994) Na+ channels must deactivate to recover from inactivation. Neuron. 12:819-829.

Kuo CC, Bean BP. (1994) Slow binding of phenytoin to inactivated sodium channels in rat hippocampal neurons. *Mol Pharmacol* **46:**716–725.

Kuo C-C, Chen R-S, Lu L, and Chen RC (1997) Carbamazepine inhibition of neuronal Na+ currents: quantitative distinction from phenytoin and possible therapeutic implications. *Mol Pharmacol* **51:**1077–1083.

Kuo C-C and Lu L (1997) Characterization of lamotrigine inhibition of Na+ channels in rat hippocampal neurons. *Br J Pharmacol* **121:**1231–1238.

Lau K, McLean WG, Williams DP, and Howard CV (2006) Synergistic interactions between commonly used food additives in a developmental neurotoxicity test. *Toxicol Sci* **90:**178–187.

Lipkind GM, Fozzard HA. (2010) Molecular model of anticonvulsant drug binding to the voltage-gated sodium channel inner pore. Mol Pharmacol.;78:631-638.

Park M, Park HR, Kim SJ, Kim MS, Kong KH, Kim HS, Gong EJ, Kim ME, Kim HS, Lee BM, and Lee J (2009) Risk assessment for the combinational effects of food color addictives: neural progenitor cells and hippocampal neurogenesis. *J Toxicol Environ Health A.* **72:**1412–1423.

Peng W, Cotrina ML, Han X, Yu H, Bekar L, Blum L, Takano T, Tian GF, Coldma SA, and Nedergaard M (2009) Systemic administration of an antagonist of the ATP-sensitive receptor P2X7 improves recovery after spinal cord injury. *Proc Natl Acad Sci USA* **106:**12489–12493.

Ragsdale DS, McPhee JC, Scheduer T, and Catterall WA (1996) Common molecular determinants of local anesthetic, antiarrhythmic, and anticonvulsant block of voltage-gated Na channels. *Proc Natl Acad Sci USA* **93:**9270–9275.

Remy M, Thaler S, Schumann RG, May CA, Fiedorowicz M, Shuettauf F, Gruterich M, Priglinger SG, Nentwich MM, Kampik A, and Haritoglou C (2008) An in vivo evaluation of briiliant blue G in animals and humans. *Br J Ophthalmol* **92:**1142-1147.

Rudy B (1978) Slow inactivation of the sodium conductance in squid giant axons. Pronase resistance. *J Physiol* **283:**1–21.

Ryu JK and McLamon JG (2008) Block of purinergic P2X(7) receptor is neuroprotective in an animal model of Alzheimer's disease. *Neuroreport* **19:**1715–1719.

Sheets PL, Heers C, Stoehr T, Cummins TR. (2008) Differential block of sensory neuronal voltage-gated sodium channels by lacosamide [(2R)-2-(acetylamino)-N-benzyl-3-methoxypropanamide], lidocaine, and carbamazepine. J Pharmacol Exp Ther. 326:89-99.

Struyk AF and Cannon SC (2002) Slow inactivation does not block the aqueous accessibility to the outer pore of voltage-gated Nav channels. *J Gen Physiol* **120:**509–516.

Ulbricht W (2005) Sodium channel inactivation: molecular determinants and modulation. *Physiol Rev.* **85**:1271–1301.

Vedantham V, Cannon SC. (1998) Slow inactivation does not affect movement of the fast inactivation gate in voltage-gated Na+ channels. J Gen Physiol. 111:83-93..

Vilin YY and Ruben PC (2001) Slow inactivation in voltage-gated sodium channels: molecular substrates and contributions to channelopathies. Cell Biochem Biophys. 35:171-90.

Waxman SG, Dib-Hajj S, Cummins TR, and Black JA (1999) Sodium channels and pain. *Proc Natl Acad Sci USA* **96:**7635–7639.

Waxman SG and Hains BC (2006) Fire and phantoms after spinal cord injury: Na+ channels and central pain. *Trends Neurosci* **29:**207–215.

West JW, Patton DE, Scheuer T, Wang Y, Goldin AL, Catterall WA. (1992) A cluster of hydrophobic amino acid residues required for fast Na(+)-channel inactivation. Proc Natl Acad Sci U S A. 89:10910-10914.

Wood JN, Boorman JP, Okuse K, and Baker MD (2004) Voltage-gated sodium channels and pain pathways. *J Neurobiol* **61:**55–71.

Xiong W, Li RA, Tian Y, Tomaselli GF. (2003) Molecular motions of the outer ring of charge of the sodium channel: do they couple to slow inactivation? J Gen Physiol. 122:323-332.

Yang YC, Kuo CC. (2002) Inhibition of Na(+) current by imipramine and related compounds: different binding kinetics as an inactivation stabilizer and as an open channel blocker. Mol Pharmacol. 62:1228-1237.

Yarov-Yarovoy V, Brown J, Sharp EM, Clare JJ, Scheuer T, Catterall WA. (2001) Molecular determinants of voltage-dependent gating and binding of pore-blocking drugs in transmembrane segment IIIS6 of the Na(+) channel alpha subunit. J Biol Chem. 276:20-27.

Footnotes

Figure Legends

Fig. 1. Block of sodium channels by BBG. A, Effect of 3 μM BBG (applied for 1 minute) on sodium current elicited by a 20-msec step from −60 mV to 0 mV. B, Time course of inhibition by 3 μM BBG. Depolarizations from −60 mV to 0 mV were delivered every 3 seconds. Solution changes were complete within 1 second. C, Dose-dependence of BBG inhibition when tested from holding potentials of −60 mV (open circles), -80 (filled circles), or -120 mV (filled squares). For applications at -60 mV or -80 mV, 1 to 100 μM BBG solutions were sequentially applied for 1 to 2 min, with wash-out for 1 to 2 min after each BBG solution. For applications at -120 mV, 3 μM, 30 μM and 100 μM BBG were sequentially applied without wash-out in between. Data points and error bars indicate mean ± SEM for measurements in 3-5 cells. Current is normalized to the initial peak current. Solid lines: best fits to $1/(1 + [BBG]/IC_{50})$, where [BBG] is the BBG concentration and IC_{50} is the half-blocking concentration. Fitted curves were drawn with $IC_{50} = 2.2$ μM for the data with a holding potential of −60 mV, $IC_{50} = 9.7$ μM for data from –80 mV, and $IC_{50} = 171$ μM for data from –120 mV. D, Reverse transcription PCR using total RNA of N1E-115 cells. The sizes of each amplified cDNA for each subtype were 331 bp (Nav1.1), 298 bp (1.2), 290 bp (1.3), 271 bp (1.4), 278 bp (1.5), 325 bp (NaX), 295 bp (1.6), 291 bp (1.7), 345 bp (1.8) and 287 bp (1.9).

Fig. 2. Use-dependent block by BBG. Sodium current was elicited by 20 ms depolarizations from −80 mV to 0 mV. Following a period of slow stimulation (every 20 seconds), the frequency was abruptly increased to 3 Hz train. The protocol was run in control conditions and then in 3 μM BBG, which reduced the current elicited by slow stimulation from 3.0 nA to 1.3 nA. Peak sodium current was normalized with reference to the current with slow stimulation in each condition.

Fig. 3. The voltage dependence of activation was not affected by BBG. A, Sodium currents were elicited by a series of voltage steps from a holding potential of −80 mV to test voltages varying from −75 mV to 0 mV in the absence or presence of 3 μM BBG. B, Current-voltage relationship for peak sodium current as a function of test pulse (different

cell than A). C, Conductance-voltage relationship in the absence (open circles) or presence (closed circles) of BBG, calculated as $G_{Na} = I_{Na}/(V-V_{rev})$, where G_{Na} is conductance, I_{Na} is current (measured at the peak), and V_{rev} is the reversal potential for sodium channel current (taken as +60 mV). Data were normalized to the maximum peak conductance and fit by the Boltzmann equation $1/(1 + \exp(-(V - V_h)/k))$, where V_h is voltage of half-maximal activation, V is test potential and k is the slope factor. Control: $V_h = -24.7$ mV, $k=3.7$ mV, BBG: $V_h = -24.4$ mV, $k=4.2$ mV.

Fig. 4. The voltage dependence of inactivation was shifted by BBG. A, Voltage dependence of inactivation determined with 1-sec conditioning pulses in various concentrations of BBG. Sodium channel availability was assayed by a test step to 0 mV following a 1 second prepulse to varying voltages. Lower to higher BBG solutions were sequentially applied for 1 to 2 min and the cell was washed with control solution for 1 to 2 min between BBG solutions. B, Collected data from 4 cells. Data from each condition in each cell were fit individually by the Boltzmann equation $1/(1 + \exp((V - V_h)/k))$, where V_h is voltage of half-maximal inactivation, V is test potential and k is the slope factor. The plotted smooth curves are drawn according to the mean V_h and slope factor for each condition (n=4 for all). Control: $V_h = -66.4 \pm 1.2$ mV, $k = 6.2 \pm 0.2$; 3 μM BBG: $V_h = -72.7 \pm 1.1$ mV, $k = 7.3 \pm 0.3$; 30 μM BBG: $V_h = -80 \pm 1.1$ mV, $k = 8.8 \pm 0.4$; 100 μM BBG: $V_h = -87 \pm 0.8$ mV, $k = 9.3 \pm 0.4$ (n = 4).

Fig 5. Effect of BBG on the time-course of recovery from inactivation. A, Inactivation was produced by a 20 ms conditioning pulse (I_c) to 0 mV and a varying time for recovery (Δt) at −80 mV was applied before a test pulse (I_t) to 0 mV. Relative I_{Na} after each recovery time was calculated as I_t divided by I_c. Points and error bars show mean ± S.E.M. for experiments in 4 cells, each with measurements in control and with 3 μM BBG. The time-course of recovery was fit with a double exponential function: $y = A_1(1 - \exp(-t/\tau_1)) + A_2(1 - \exp(-t/\tau_2))$ where t is time, A_1 and A_2 are the coefficients for the fast and slow exponentials, and τ_1 and τ_2 are the fast and slow time constants. Control: τ_{fast} 4.9 ± 0.4 msec, τ_{slow} 57.5 ± 11.4 msec: τ_{fast} 7.2 ± 0.8 msec, τ_{slow} 94 ± 16 msec. B, Time course of recovery following a 10-second conditioning pulse to 0 mV, tested with a 20-msec test

pulse to 0 mV at varying times after return of the voltage to -120 mV. Test currents were normalized to the largest current elicited by the step to 0 mV in each condition.

Fig. 6. BBG enhancement of slowly-recovering channels. A, Slow inactivation was measured by applying a 5-second depolarization to varying voltages (from a steady holding potential of -120 mV), returning to -120 mV for 100 msec to allow recovery from fast inactivation, and delivering a test step to 0 mV. Test currents were normalized to the maximal test current elicited in each condition (after a conditioning pulse to -140 mV). Open circles, control; closed circles, 3 μM BBG, open squares 30 μM BBG, closed triangles 100 μM BBG. Data are fit by a modified Boltzmann function: $I/I_{max} = (1 - I_{resid})/((1 + \exp((V_m - V_h)/k)) + I_{resid}$. Control: $V_h = -34$ mV, $k=24$ mV, $I_{resid} = 0.76$. 3 μM BBG: $V_h = -58$ mV, $k=16$ mV, $I_{resid} = 0.13$. 30 μM BBG: $V_h = -84$ mV, $k=14$ mV, $I_{resid} = 0.08$. 100 μM BBG: $V_h = -95$ mV, $k=13$ mV, $I_{resid} = 0.03$. B, Time course of entry into slowly-recovering states at -50 mV (left) and 0 mV (right). A step to either -50 mV or 0 mV varying in length from 1 to 16 seconds was given from a holding potential of -120 mV. A 100-msec interval at -120 mV then allowed for recovery of fast-inactivated channels, and the fraction of channels remaining in slowly-recovering states was assayed by a pulse to 0 mV. Solid curves: best fits of single exponential functions decaying to a steady-state. At -50 mV, Control: $\tau = 16.7$ s, steady-state 0.8; 3 μM BBG: $\tau = 10.6$ s, steady-state 0.2; 30 μM BBG: $\tau = 1.3$ s, steady-state 0.2; 100 μM BBG: $\tau = 0.85$ s, steady-state 0.1. At 0 mV, Control: $\tau = 13.6$ s, steady-state 0.5; 3 μM BBG: $\tau = 1.9$ s, steady-state 0.1; 30 μM BBG: $\tau = 0.71$ s, steady-state 0.1; 100 μM BBG: $\tau = 0.59$ s, steady-state 0.

Fig. 7. Kinetic model for BBG interaction with sodium channels. A, Model. BBG is hypothesized to bind weakly (with 1:1 stoichiometry) to the resting closed state R, more tightly to the fast-inactivated state I, and more tightly yet to the slow-inactivated state S. For BBG binding and unbinding to R, the on-rate (konR) was 0.000118 ms^{-1} μM^{-1} and off-rate (koffR) was 0.02 ms^{-1}. For BBG binding and unbinding to I, konI= 0.0001 ms^{-1} μM^{-1} and koffI= 0.0005 ms^{-1}. For BBG binding and unbinding to S, konS= 0.001 ms^{-1} μM^{-1} and koffS= 0.0002 ms^{-1}. Channels moved between R and I with a forward rate

constant given by $1/(1+\exp(-(V+50)/8))$ ms^{-1} and a back rate constant of $0.18/(1+\exp((V+60)/8))$ ms^{-1} and channels moved between I and S with a forward rate constant of $0.0001/(1+\exp(-(V+25)/16))$ ms^{-1} and back rate constant of $0.0008/(1+\exp((V+25)/16))$ ms^{-1}, where V is voltage. To preserve microscopic reversibility, the rate constant for movement from IB to RB was multiplied by a factor of (koffI/koffR)*(konR/konI) relative to that for I to R and the rate constant for movement from IB to SB was multiplied by a factor of (konS/konI)*(koffI/koffS) relative to that for I to S. The model was implemented in IgorPro (Wavemetrics, Lake Oswego, OR) using fourth-order Runge-Kutta integration with a 200-μs step size.

B, Predictions of model for sodium channel availability (fraction of channels in state R) after 1-sec conditioning pulses. As for experimental data, availability in each condition is normalized to the maximal availability following a prepulse to -120 mV. Solid lines show fits of Boltzmann functions with the indicated midpoints. C, Predictions of model for recovery of available channels at -120 mV following a 10-sec conditioning pulse to 0 mV, according to the protocol in Fig. 5B. Availability in each concentration of BBG is normalized to the steady-state availability at -120 mV. D, Predictions of model for entry into slowly-recovering states during 5-sec depolarizations to a range of voltages. The Y axis plots relative fraction of channels in either state R or state I (which would be available following 100 msec recovery at -120 mV, as in Fig. 6A). Normalization is to the maximal fraction in R or I in each condition, at -120 mV. E, Predictions of model for kinetics of entry into slowly-recovering states during conditioning pulses to either -50 mV (left) or 0 mV (right). Y axes plot relative fraction of channels in either state R or state I and normalization is to the maximal fraction in R or I in each condition.

Fig. 8. Minimal effect of Brilliant Blue FCF on sodium channels. A, Effect of 30 μM Brilliant Blue FCF applied during stimulation at 0.33 Hz (with 20-msec steps from -80 mV to 0 mV). B, Voltage dependence of inactivation in absence and presence of 30 μM Brilliant Blue FCF (n = 3). Control: V_h= −66 mV ± 0.6, k=6.6 ± 0.13; 30 μM Brilliant Blue FCF: V_h= −68.4 mV ± 1.1, k=6.8 ± 0.3 (n = 3). Inactivation was measured using 1-sec prepulses followed by a test step to 0 mV (same protocol as Figure 4, where 30 μM BBG produced a shift from V_h = −66.4 ± 1.2 mV, k = 6.2 ± 0.2 to V_h = −80 ± 1.1 mV, k =

8.8 ± 0.4). C, Voltage dependence of slow inactivation in control and with 30 μM Brilliant Blue FCF (n = 3). Slow inactivation was measured by applying a 5-second depolarization to varying voltages, returning to −80 mV for one second to allow complete recovery from fast inactivation, and then assaying channel availability with a test pulse to 0 mV. Control: Reduction to 72 ± 3 % at -10 mV, midpoint -46 ± 6 mV, slope factor 25 ± 4 mV. 30 μM Brilliant Blue FCF: Reduction to 67 ± 2% at -10 mV, midpoint -48 ± 3 mV, slope factor 21 ± 2 mV. The effect of 10-fold lower (3 μM) BBG using the same protocol (in a different set of 4 cells) was much larger (not shown): Control: Reduction to 70 ± 3 % at -10 mV, midpoint -59 ± 2 mV, slope factor 19 ± 0.4 mV. 3 μM BBG: Reduction to 36 ± 4% at -10 mV, midpoint -70 ± 3 mV, slope factor 15 ± 1 mV (n=4). D, Recovery from slow inactivation (n = 3). Recovery from slow inactivation was measured by a series of brief (20 msec) test pulses to 0 mV after a long 5-second conditioning pulse to −20 mV followed by return to −80 mV for variable times. Control: τ_{fast}=6.3 ± 0.7 ms, τ_{slow}=0.7 ± 0.1 sec, slow fraction = 28 ± 2%; Brilliant Blue FCF: τ_{fast}=7.8 ± 0.8 ms, τ_{slow}=0.6 ± 0.6 sec., slow fraction = 29 ± 2 %. The effect of 3 μM BBG using the same protocol was much larger (not shown): Control: τ_{fast}=6.5 ± 0.6 ms, τ_{slow}=0.8 ± 0.7 sec, slow fraction = 33 ± 7%; 3 μM BBG: τ_{fast}=13 ± 2.6 ms, τ_{slow}=0.9 ± 0.5 sec, slow fraction = 76 ± 4% (n=4).

Figure 1

Figure 2

A

mV
0
-40
-80

Control

1 nA

2 ms

3 μM BBG

1 nA

2 ms

B

Peak I_{Na} (nA)

V (mV)

○ Control
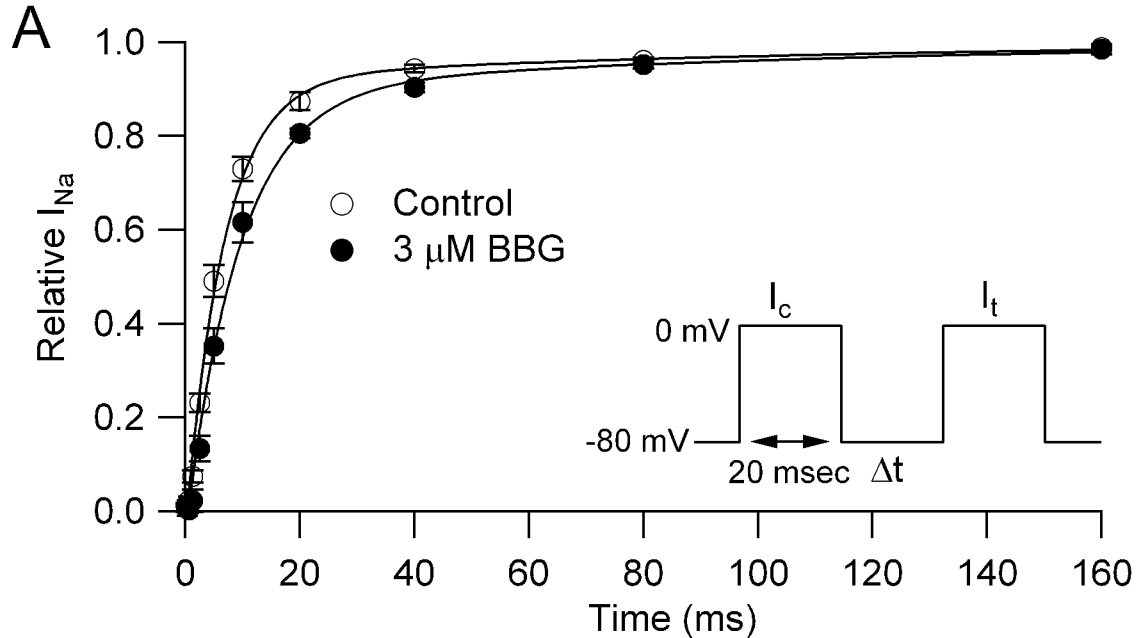● 3 μM BBG

C

Relative G_{Na}

○ Control
● BBG

V (mV)
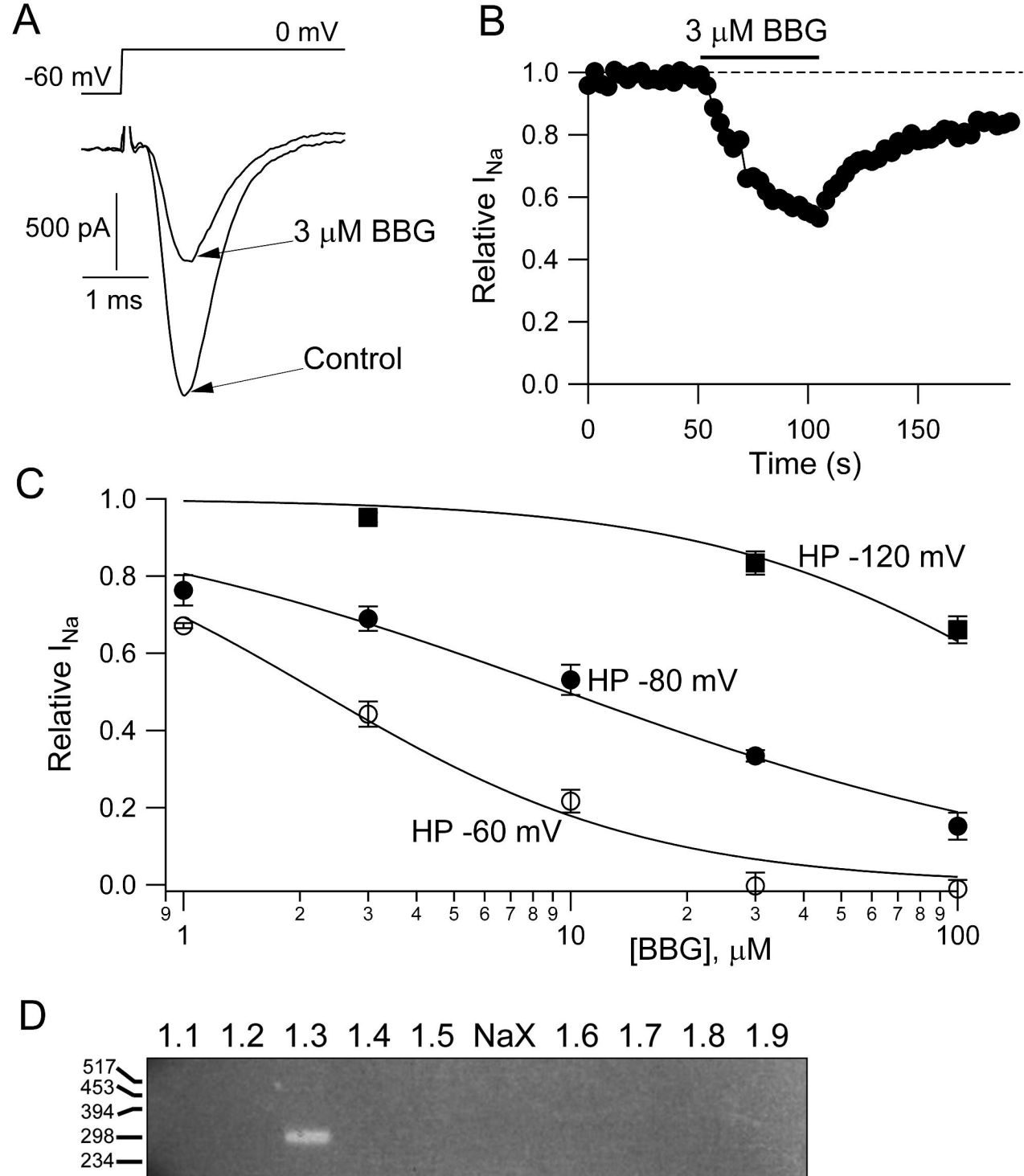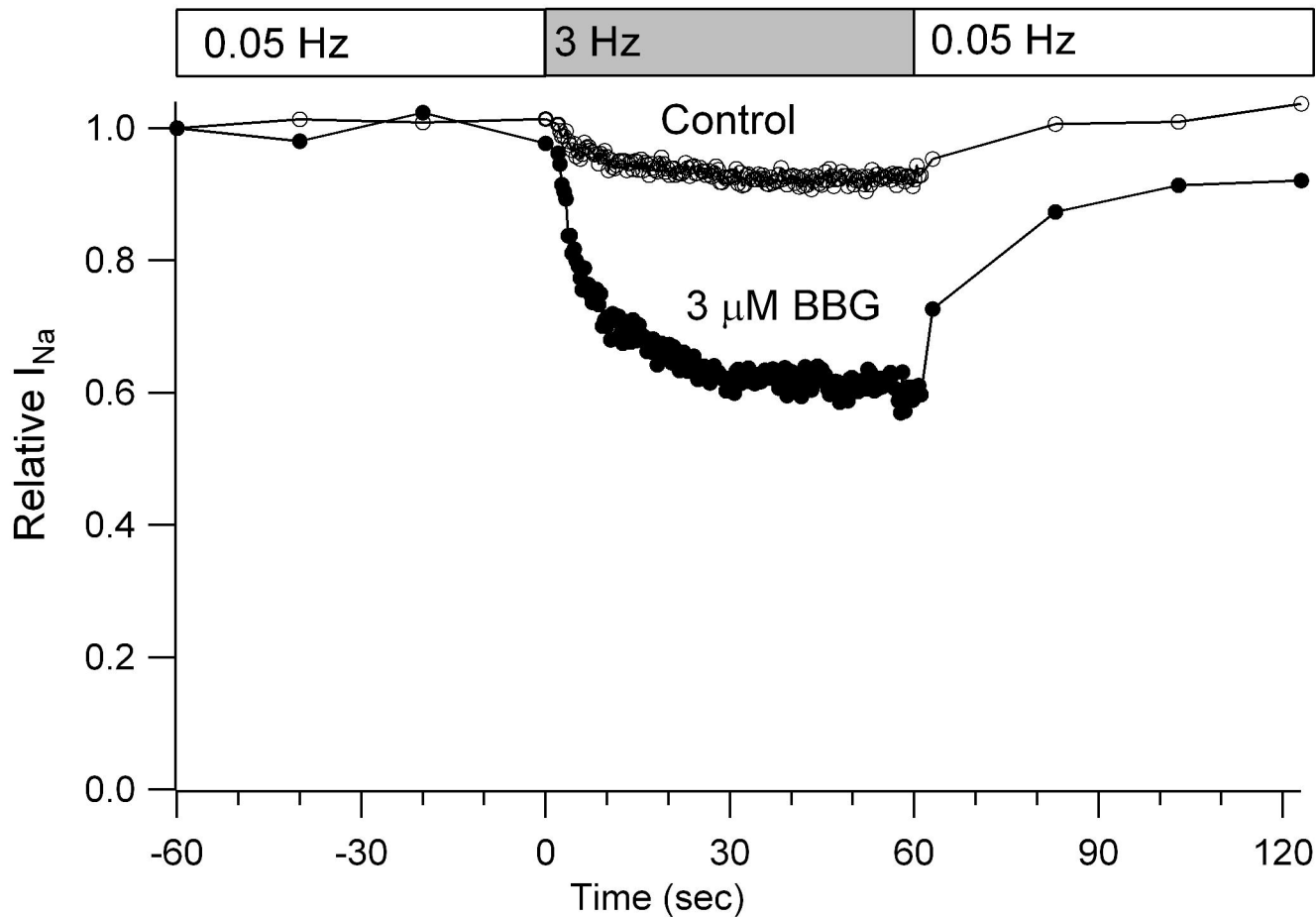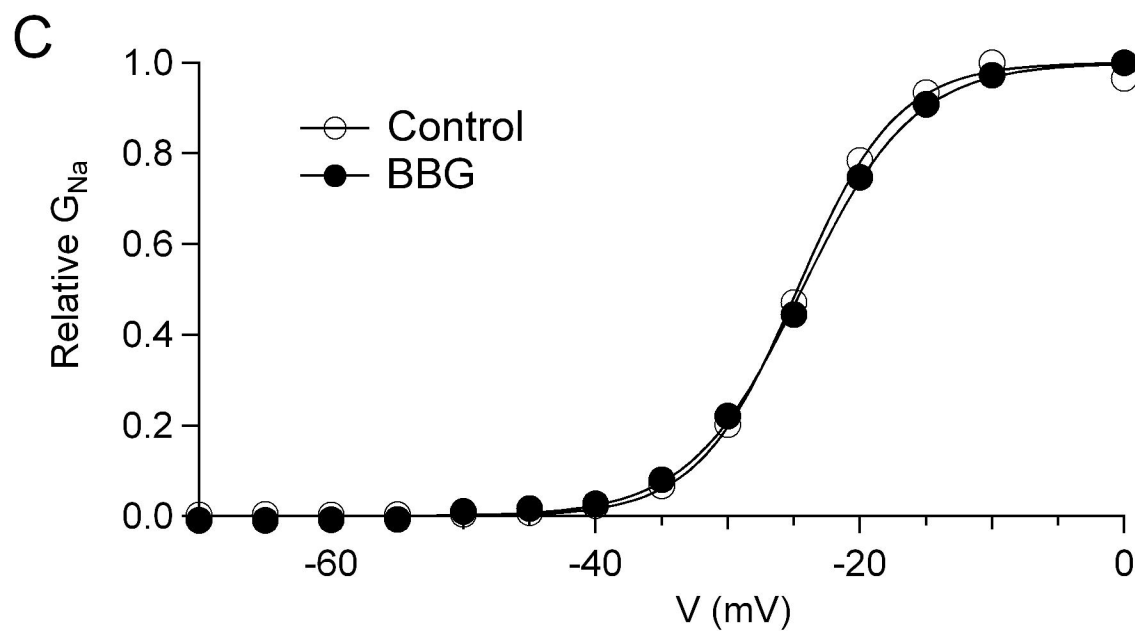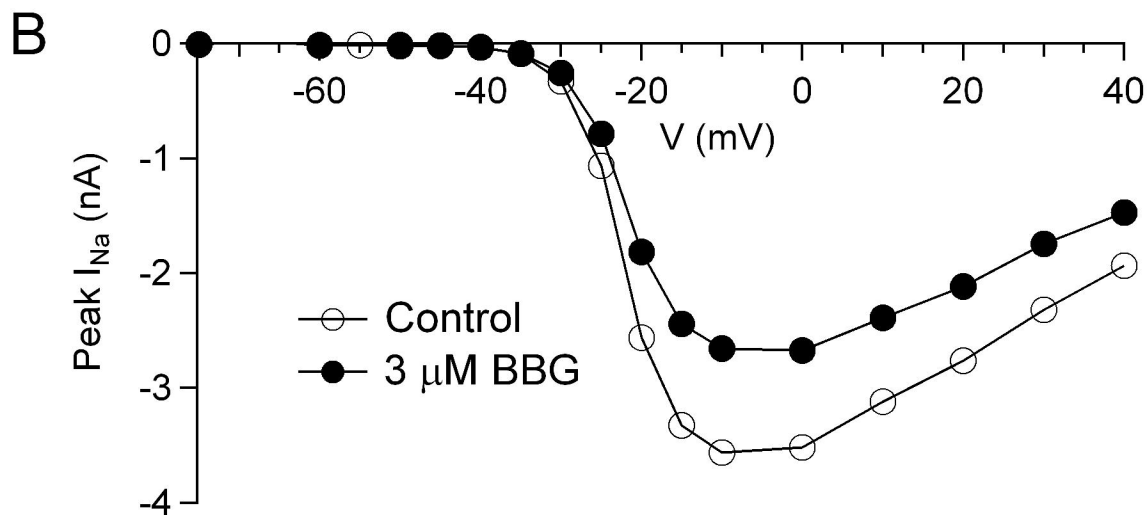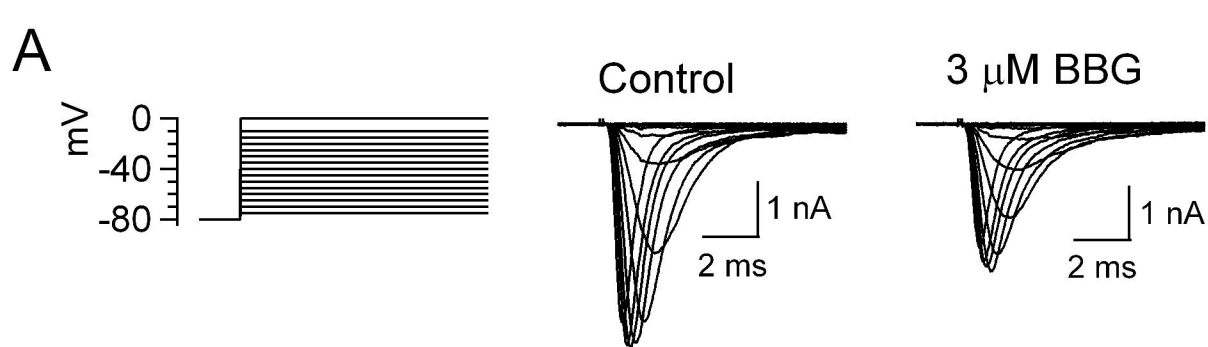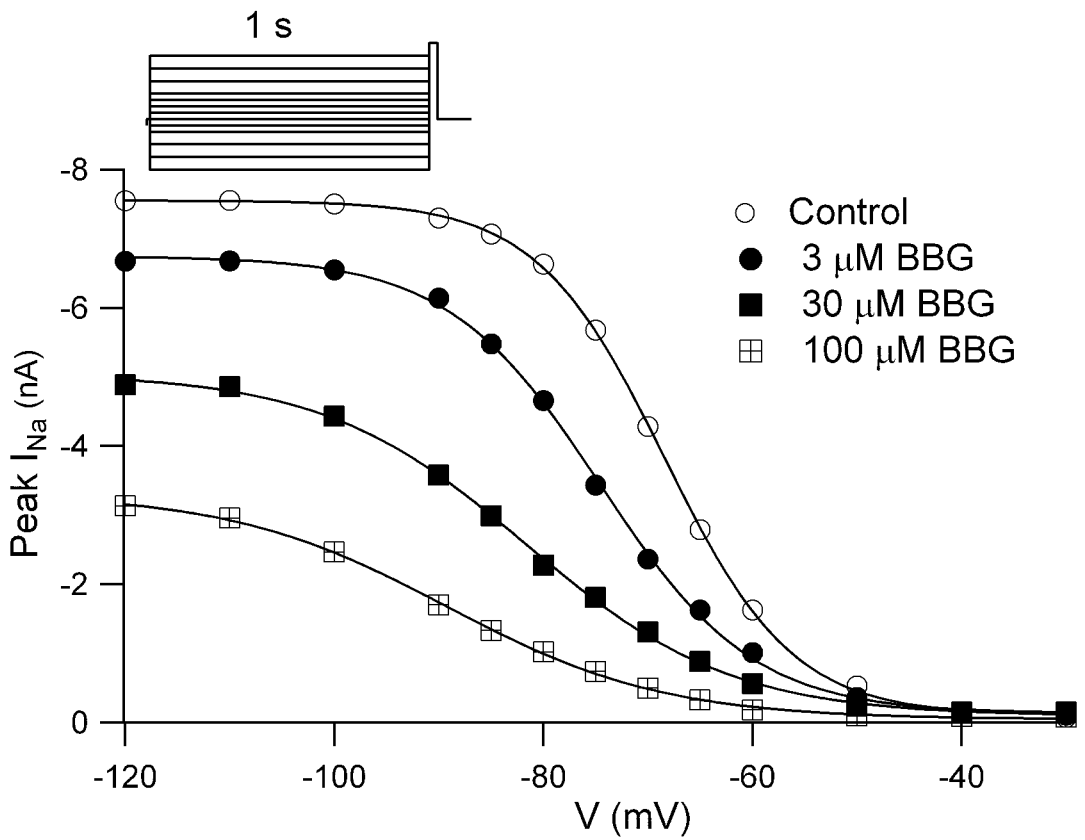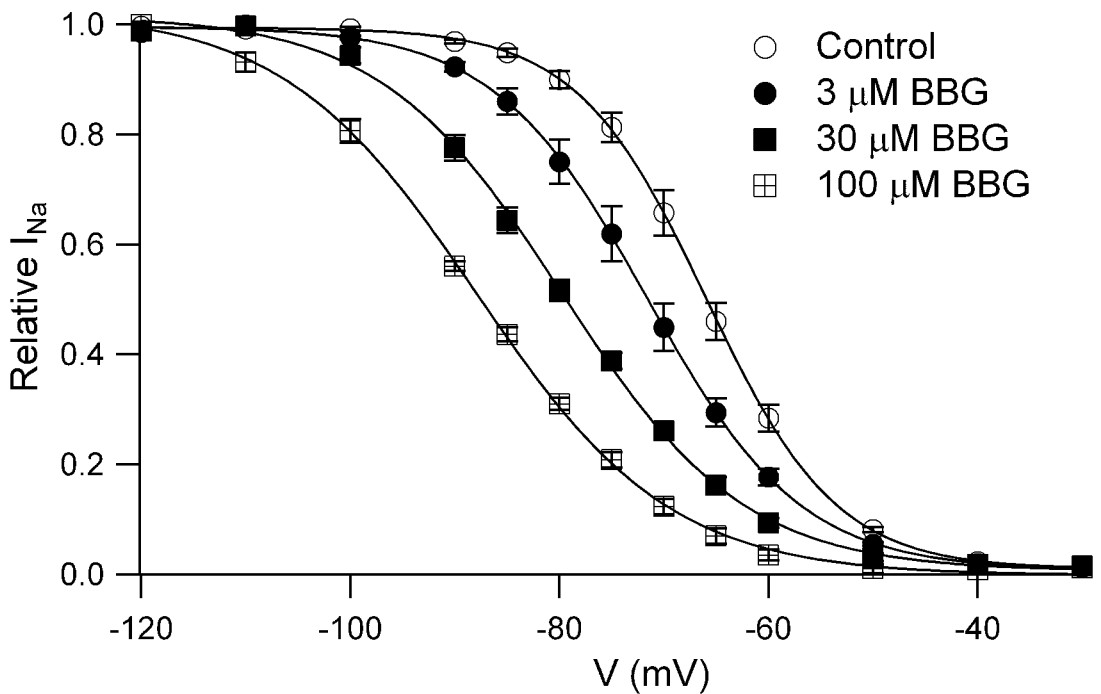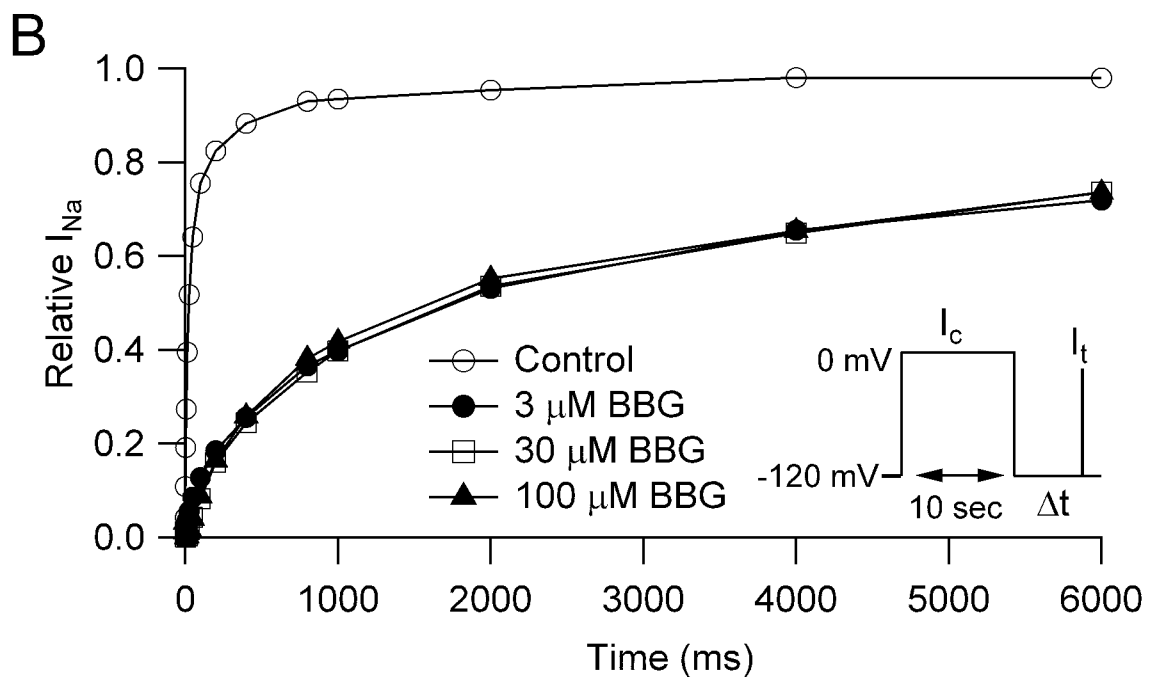
Figure 3
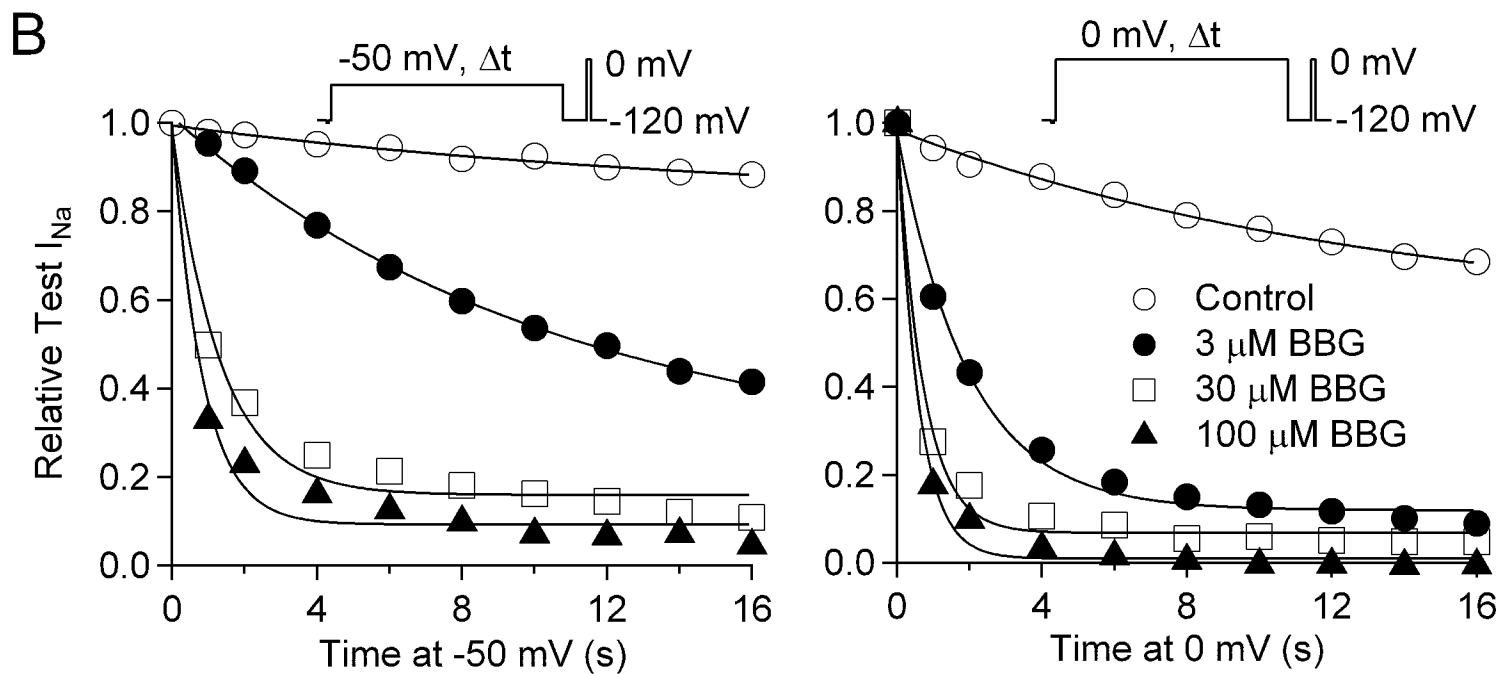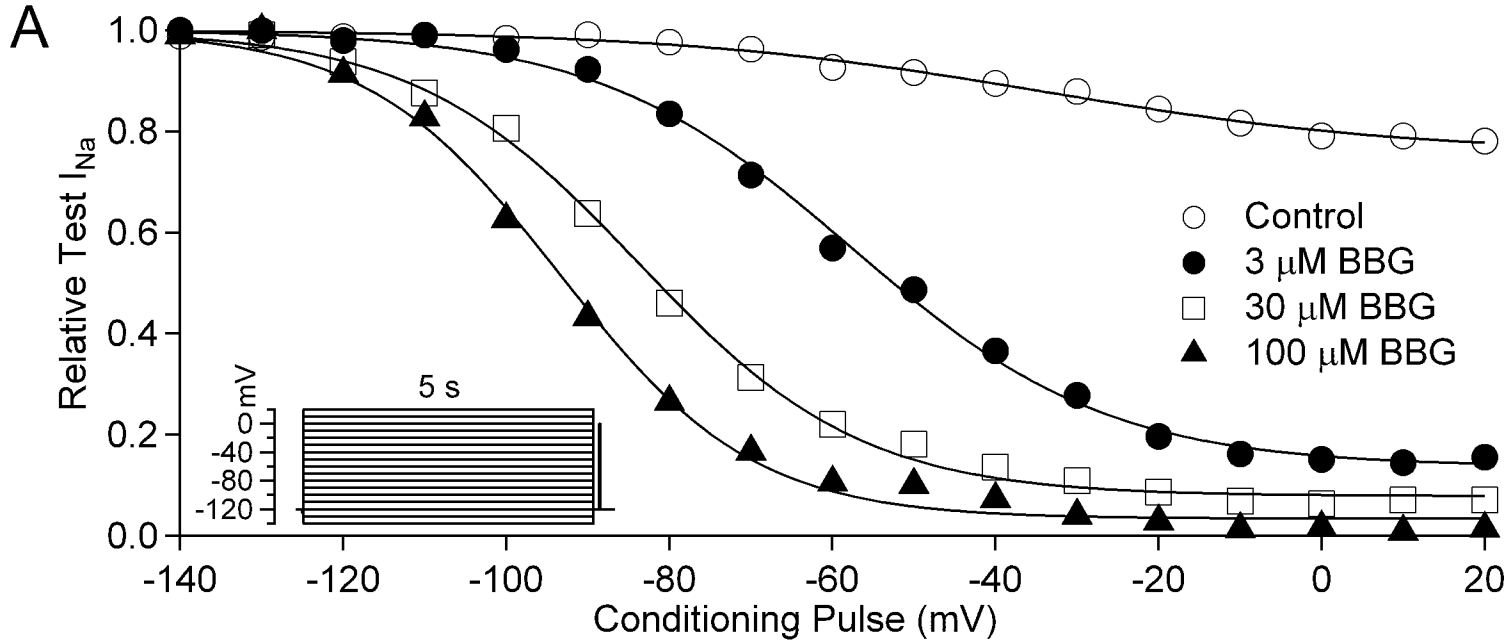
Figure 4

Figure 5

Figure 6

Figure 7

Figure 8